PHYSICAL REVIEW D **93,** 074019 (2016)

Searching for vector dark matter via Higgs portal at the LHC

Chuan-Hung Chen* and Takaaki Nomura†

Department of Physics, National Cheng-Kung University, Tainan 70101, Taiwan

(Received 20 February 2016; published 18 April 2016)

A Higgs portal dark matter model for explaining the gamma ray excess from the galactic center can be realized with the extension of local $SU(2)_X$ gauge symmetry with one quadruplet. Due to the residual Z_3 discrete symmetry of $SU(2)_X$, the new gauge bosons are the stable dark matter candidates. Due to the mixture of the standard model Higgs doublet and the introduced quadruplet, dark matter could annihilate into the standard model particles through the Higgs portal and new scalar portal. We study the discovery significance of the vector dark matter at the Large Hadron Collider. The involved parameters are consistent with the constraints from relic density and direct detection and with the data of the galactic center gamma ray excess. With $\sqrt{s} = 14$ TeV and luminosities of 100 and 300 fb^{-1}, we find that a discovery significance of $S/\sqrt{B} = 5$ can be easily reached if the production of dark matter is through the invisible decays of the Higgs boson and a new scalar boson.

DOI: 10.1103/PhysRevD.93.074019

I. INTRODUCTION

Clear evidence of new physics can be based on two measurements, namely neutrino oscillations, which lead to massive neutrinos [1] and astronomical evidence of dark matter (DM), where the weakly interacting massive particles (WIMPs) are the candidates in particle physics.

Although the direct detection of WIMPs in the LUX experiment [2] has put a strict limit on the couplings and mass of DM, potential DM signals are indicated by the indirect detections, such as the positron excess, which was uncovered by PAMELA [3] and Fermi-LAT [4]. With measurements of unprecedented precision, the AMS Collaboration further confirmed the excess of the positron fraction in the range from 0.5 to 500 GeV [5] and of the positron + electron flux from 0.5 GeV to 1 TeV [6]. Nevertheless, there are possible explanations for the cosmic ray excess, such as pulsars [7,8] and the propagation of cosmic rays from a secondary origin [9].

A clear excess of the gamma ray spectrum, which has a peak at the photon energy of around 2 GeV, has recently been found [10–17]. Using the data of the Fermi Gamma-ray Space Telescope [18,19], a significant signal of gamma rays from the region around the galactic center has been found [20–24]. An interesting finding is that the gamma ray excess can be interpreted well by DM annihilation and that the associated thermally averaged cross section $\langle \sigma v_{\rm rel} \rangle$ is on the order of 10^{-26} cm^3/s, which is the same as that for the thermal relic density. Unlike the case of positron cosmic rays, a boost factor is unnecessary for the excess of the gamma ray spectrum. Therefore, the gamma ray spectrum is a more promising clue for verifying WIMPs as DM candidates.

With WIMPs considered as DM candidates, it is of interest to determine what effect guarantees the stability of DM and what mediator connects the dark side and visible side. To protect DM from decay, a dark charge associated with an unbroken symmetry is necessary in the theory; this charge is usually added to models. Regarding stability, we assume that an unbroken discrete symmetry can be the remnant of a local gauge symmetry, which is broken spontaneously. According to previous analysis [20,25–28], a plausible mechanism for the mediator could be through the Higgs portal [29]. The Higgs boson, the last discovered piece in the standard model (SM) and whose mass is 125 GeV, has been measured recently by ATLAS [30] and CMS [31]. In this work, we investigate a model in which the dark charge is the residual symmetry of a gauge group and in which the SM Higgs boson and a new scalar boson are the messengers between dark and visible sectors.

To realize this model, we assume that the DM candidates do not belong to the multiplet of the SM gauge symmetry group but are the states of an extra hidden local $SU(2)_X$ gauge symmetry, where X can be regarded as the quantum number of dark charge. Since the local gauge symmetry must accompany gauge bosons, without further introducing new degrees of freedom, it is plausible to require the new gauge bosons to be the DM candidates. Moreover, in order to have a residual discrete symmetry when the local $SU(2)_X$ is broken spontaneously, we find that our intentions can be achieved easily if a quadruplet of $SU(2)_X$ is employed. As a result, a Z_3 discrete symmetry of $SU(2)_X$ remains in the ground state when the quadruplet gets a vacuum expectation value (VEV) [32]. Additionally, the introduced quadruplet is not only responsible for the breaking of $SU(2)_X$ but also plays an important role in the communication between dark and visible sectors. Detailed studies of the model and its implications on relic

*physchen@mail.ncku.edu.tw
†nomura@mail.ncku.edu.tw

density and the gamma ray excess of the galactic center can be found elsewhere [32]. Other approaches for stabilizing the DM in $SU(2)_X$ have been proposed [33–39].

Besides direct and indirect DM detection, high-energy colliders, e.g., Large Hadron Collider (LHC), could also provide signals of DM. Such searches depend on the mass of DM and the associated couplings. For $m_\chi < m_h/2$, when DM is produced by the on-shell SM Higgs boson, the invisible Higgs decays will directly give a strict constraint on the involved couplings [40–43]. For heavier DM, although the constraint from invisible Higgs decays can be avoided, there is a lower production cross section [44,45]. For explaining the gamma ray excess through DM annihilation, the preferred scale of DM mass is less than the W-gauge boson [24,32]; therefore, we focus on the lighter DM with $m_\chi < m_W$. In this model, there exists another scalar boson, which is from the quadruplet of $SU(2)_X$. Since the new scalar boson mixes with the SM Higgs, its properties are similar to those of the SM Higgs. We also study its influence on the DM production at colliders.

Based on the vector DM model, which is dictated by an extra local $SU(2)_X$ gauge symmetry [32], we study the Higgs portal vector DM signals at the $\sqrt{s} = 14$ TeV LHC. Besides the background analysis, we discuss each channel that produces the DM signal. The potential channels include (a) vector boson fusion (VBF), $pp \to S^{(*)}jj$, (b) monojet, $pp \to S^{(*)}j$, (c) mono-W/Z, $pp \to S^{(*)}W/Z$, and (d) $t\bar{t}$, $pp \to S^{(*)}t\bar{t}$, where $S^{(*)}$ denotes the on-shell or off-shell Higgs boson and the new scalar boson. We find that the monojet and VBF channels dominate the DM production cross section, with the other channels having a relatively small contribution. After considering the kinematic cuts for reducing the backgrounds, the ratio of the signal to the background from the monojet is smaller than that from VBF. Therefore, we study the VBF process in detail.

The rest of this paper is organized as follows. Section II briefly introduces the WIMP model and summarizes the couplings of DM to the SM Higgs boson and to the new scalar boson. Section III discusses the constraints of parameters, introduces the signals and possible backgrounds, and analyzes the cross section for each signal channel. We introduce proper kinematic cuts and simulate the signal and background events in Sec. IV. In addition, we discuss the discovery significance as a function of parameters in this section. Conclusions are given in Sec. V.

II. WIMPS IN HIDDEN $SU(2)_X$ AND THEIR COUPLINGS WITH HIGGS

A. WIMPs

This section briefly introduces the WIMP model and discusses the relevant interactions with DM candidates. For studying the minimal extension of the SM that incorporates DM, besides the SM particles and their associated gauge symmetry, we consider a new local $SU(2)_X$ gauge symmetry and add one quadruplet of $SU(2)_X$ to the model. Thus, the Lagrangian in $SU(2)_X \times SU(2)_L \times U(1)_Y$ is written as

$$\mathcal{L} = \mathcal{L}_{\rm SM} + (D_\mu \Phi_4)^\dagger D^\mu \Phi_4 - V(H, \Phi_4) - \frac{1}{4} X^a_{\mu\nu} X^{a\mu\nu} \quad (1)$$

with

$$V(H, \Phi_4) = \mu^2 H^\dagger H + \lambda (H^\dagger H)^2 + \mu_\Phi^2 \Phi_4^\dagger \Phi_4 + \lambda_\Phi (\Phi_4^\dagger \Phi_4)^2 + \lambda' \Phi_4^\dagger \Phi_4 H^\dagger H, \quad (2)$$

where $\mathcal{L}_{\rm SM}$ is the Lagrangian of the SM, $H^T = (G^+, (v + \phi + iG^0)/\sqrt{2})$ is the SM Higgs doublet, $\Phi_4^T = (\phi_{3/2}, \phi_{1/2}, -\phi_{-1/2}, \phi_{-3/2})/\sqrt{2}$ is the quadruplet of $SU(2)_X$, the index i of ϕ_i stands for the eigenvalue of the third generator of $SU(2)_X$, and $\phi_{-i} = \phi_i^*$. The covariant derivative of Φ_4 is $D_\mu = \partial_\mu + i g_X T^a X^a_\mu$, and the representations of T^3 is given by $T^3 = {\rm diag}(3/2, 1/2, -1/2, -3/2)$. The $T^{1,2}$ can be found elsewhere [32]. Since the SM is well known, it is not presented here explicitly.

For breaking the $SU(2)_X$ and preserving a discrete symmetry, the nonvanishing VEV and the associated fields that fluctuate around the VEV are set to

$$\langle \phi_{\pm 3/2} \rangle = \frac{v_4}{\sqrt{2}}, \qquad \phi_{\pm 3/2} = \frac{1}{\sqrt{2}} (v_4 + \phi_r \pm i\xi). \quad (3)$$

With the breaking pattern in Eq. (3), one can find that a Z_3 symmetry $U_3 \equiv e^{iT^3 4\pi/3} = {\rm diag}(1, e^{i2\pi/3}, e^{-2i\pi/3}, 1)$ is preserved by the ground state $\Phi_0 = (v_4/2, 0, 0, v_4/2)$. Under Z_3 transformation, the scalar fields of the quadruplet are transformed as

$$\phi_{\pm 3/2} \to \phi_{\pm 3/2}, \qquad \phi_{\pm 1/2} \to e^{\pm i2\pi/3} \phi_{\pm 1/2}. \quad (4)$$

That is, $\phi_{\pm 3/2}$ are Z_3 blind while $\phi_{\pm 1/2}$ carry the charge of Z_3. In terms of the physical states of gauge fields, one can write

$$T^a X^a_\mu = \frac{1}{\sqrt{2}} (T^+ \chi_\mu + T^- \overline{\chi}_\mu) + T^3 X^3_\mu, \quad (5)$$

with $T^\pm = T^1 \pm iT^2$ and $\chi_\mu(\overline{\chi}_\mu) = (X^1_\mu \mp iX^2_\mu)/\sqrt{2}$, where $\overline{\chi}_\mu$ is regarded as the antiparticle of χ_μ. The transformations of gauge fields are [32]

$$X_\mu^3 \to X_\mu^3,$$
$$\chi_\mu(\overline{\chi}_\mu) \to e^{\mp i2\pi/3}\chi_\mu(\overline{\chi}_\mu). \quad (6)$$

It can be seen that $\phi_{\pm 1/2}$ and $\chi_\mu(\overline{\chi}_\mu)$ carry the charges of Z_3. Since the masses of χ_μ and $\overline{\chi}_\mu$ arise from the spontaneous symmetry breaking of Φ_4, $\phi_{\pm 1/2}$ must be the Nambu-Goldstone bosons and are the longitudinal degrees of freedom of χ_μ and $\overline{\chi}_\mu$. Hence, χ_μ and $\overline{\chi}_\mu$ are the candidates of DM in the model.

B. Relationships of parameters and couplings to WIMPs

In this section, we discuss the new free parameters and their relationships. The new free parameters only appear in the new gauge sector and scalar potential shown in Eq. (2). They are g_X, μ_Φ^2, λ_Φ, and λ'. In terms of the SM Higgs doublet and quadruplet of $SU(2)_X$ and the scalar potential, the mass matrix for SM Higgs ϕ and new scalar ϕ_r is expressed as

$$M^2 = \begin{pmatrix} m_\phi^2 & \lambda' v v_4 \\ \lambda' v v_4 & m_{\phi_r}^2 \end{pmatrix}, \quad (7)$$

with $m_\phi = \sqrt{2\lambda}v$ and $m_{\phi_r} = \sqrt{2\lambda_\Phi}v_4$. Clearly, λ' causes the mixture of Higgs doublet H and quadruplet Φ_4. The mixing angle connecting the mass eigenstates can be parametrized as

$$\begin{pmatrix} h \\ H^0 \end{pmatrix} = \begin{pmatrix} \cos\theta & \sin\theta \\ -\sin\theta & \cos\theta \end{pmatrix}\begin{pmatrix} \phi \\ \phi_r \end{pmatrix}, \quad (8)$$

where h denotes the SM-like Higgs boson, H^0 is the second scalar boson and $\tan 2\theta = 2\lambda' v v_4/(m_{\phi_r}^2 - m_\phi^2)$. According to Eq. (7), the eigenvalues of the mass square matrix are found as

$$m_{h,H^0}^2 = \frac{1}{2}\left(m_\phi^2 + m_{\phi_r}^2 \pm \sqrt{(m_\phi^2 - m_{\phi_r}^2)^2 + 4\lambda'^2 v^2 v_4^2}\right). \quad (9)$$

We note that the mass of h can be larger or less than that of H^0. In addition, from the kinetic term of Φ_4, the masses of gauge bosons can be obtained as $m_\chi = \sqrt{3}g_X v_4/2$ and $m_{X^3} = \sqrt{3}m_\chi$. Hence, the set of new free parameters can be chosen as

$$\{g_X, m_\chi, m_{H^0}, \theta\}. \quad (10)$$

The mixing angle θ is constrained by the Higgs boson search at the LEP and the LHC. A thorough analysis [46] has provided the constraint as a function of the second scalar boson mass. The constraints are taken into account in the analysis of discovery significance below.

Next, we discuss the couplings of DM in the model. Since the DM candidates are the gauge bosons, their couplings to the visible sector are through the mixture of $SU(2)_X$ quadruplet and the SM Higgs doublet. Therefore, the main interactions of DM are from the kinetic term of Φ_4. With the mixing angle defined in Eq. (8), the relevant interactions are given as [32]

$$I_{\chi\overline{\chi}} = \sqrt{3}g_X m_\chi(s_\theta h + c_\theta H^0)\chi_\mu\overline{\chi}^\mu + \frac{1}{2}\left(\frac{3g_X^2}{2}\right)(s_\theta h + c_\theta H^0)^2\chi_\mu\overline{\chi}^\mu, \quad (11)$$

with $c_\theta = \cos\theta$ and $s_\theta = \sin\theta$. With these interactions, it can be seen that if $m_h > 2m_\chi$, then the invisible Higgs decay $h \to \chi\overline{\chi}$ will give a strict limit on $\sin\theta$. Besides the gauge interactions, we also derive the triple scalar couplings, expressed as

$$I_S = \frac{1}{2}(6\lambda v c_\theta^2 s_\theta + \lambda' v_4 c_\theta^3)hhH^0 + \frac{1}{2}(-6\lambda_\Phi v_4 c^2\theta s_\theta + \lambda' v c_\theta^3)hH^0H^0. \quad (12)$$

Since the mixing angle θ is related to the parameter λ', the two terms in each triple interaction should be the same in terms of their order of magnitude. If the mixing angle is not suppressed, H^0 with $m_{H^0} > m_h/2$ or $m_{H^0} < m_h/2$ through the decay $H^0 \to hh$ or $h \to H^0H^0$ has an interesting effect on the production of DM. However, since the mixing angle is constrained by DM direct detection and the effects of triple couplings on the production of DM pairs are small, we do not further discuss their contributions in this paper.

III. SIGNALS AND BACKGROUNDS

In this section, we explore the possible DM signals and backgrounds in our model. In order to estimate the cross sections of signal processes, we firstly discuss various constraints of free parameters and then introduce the possible signals and backgrounds.

A. Constraints of free parameters

By Eq. (11), we see that the vector DM candidates only couple to SM Higgs h and new scalar H^0. For producing a pair of DM particles, h and H^0 could be both off shell and on shell. For the off-shell case, the effect is directly related to the magnitude of couplings, and the main constraints are from DM relic density and DM direct detection. For the on-shell case, besides the constraints mentioned above, the invisible Higgs decay also gives a strong bound. For presenting the constraint from the invisible Higgs decay, we formulate the partial decay rate for $h(H^0) \to \chi\chi$ with $m_{h(H^0)} > m_\chi/2$ as

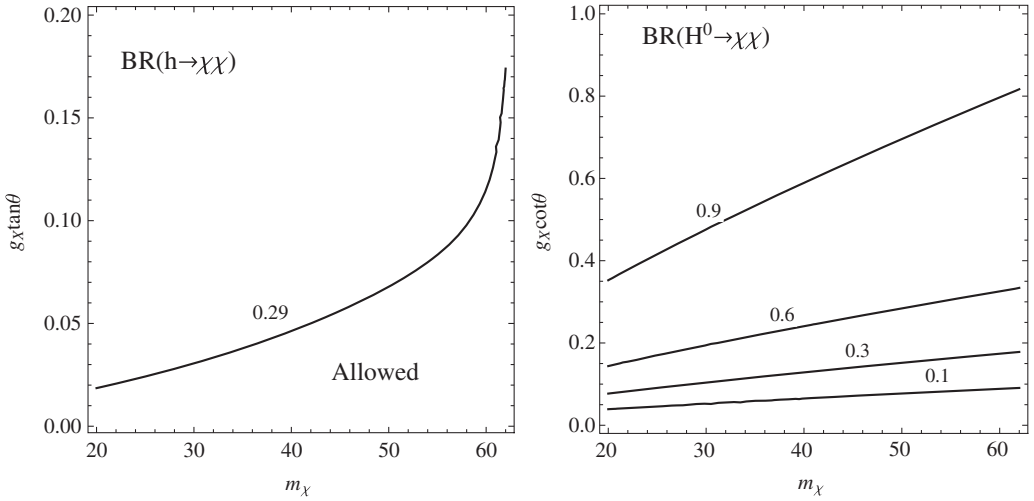

FIG. 1. Contours for invisible decay of SM Higgs h (left) and of new scalar boson H^0 (right) as a function of $g_X \tan\theta (g_X \cot\theta)$ and m_χ, where $m_h = 125$ GeV [30,31], $\Gamma_{h\to \mathrm{SM}} = 4.21$ MeV [47], and the measurement of $\mathrm{BR}(h \to \chi\chi) < 0.29$ [48] is used. In $H^0 \to \chi\chi$, we assume $m_{H^0} = 2m_\chi + 1$.

$$\Gamma(S \to \chi\bar{\chi}) = \frac{3g'^2}{64\pi m_S} \frac{m_S^4 - 4m_\chi^2 m_S^2 + 12m_\chi^4}{m_\chi^2} \left(1 - \frac{4m_\chi^2}{m_S^2}\right)^{1/2}, \tag{13}$$

where $g' = g_X s_\theta (g_X c_\theta)$ when $S = h(H^0)$. The branching ratios (BRs) of the invisible decays can be expressed as

$$\begin{aligned} \mathrm{Br}(h \to \chi\bar{\chi}) &= \frac{\Gamma_{h\to\chi\bar{\chi}}}{\Gamma_{h\to\chi\bar{\chi}} + \Gamma_{h\to \mathrm{SM}} c_\theta^2} \\ &= \frac{\Gamma_{h\to\chi\bar{\chi}}^{g'=1} (g_X \tan\theta)^2}{\Gamma_{h\to\chi\bar{\chi}}^{g'=1} (g_X \tan\theta)^2 + \Gamma_{h\to \mathrm{SM}}}, \end{aligned} \tag{14}$$

$$\begin{aligned} \mathrm{Br}(H^0 \to \chi\bar{\chi}) &= \frac{\Gamma_{H^0\to\chi\bar{\chi}}}{\Gamma_{H^0\to\chi\bar{\chi}} + \Gamma_{h\to \mathrm{SM}}^{m_{H^0}} s_\theta^2} \\ &= \frac{\Gamma_{H^0\to\chi\bar{\chi}}^{g'=1} (g_X \cot\theta)^2}{\Gamma_{H^0\to\chi\bar{\chi}}^{g'=1} (g_X \cot\theta)^2 + \Gamma_{h\to \mathrm{SM}}^{m_{H^0}}}, \end{aligned} \tag{15}$$

with $\Gamma_{h\to \mathrm{SM}}$ being the width of the SM Higgs. The expression of $\Gamma_{h\to \mathrm{SM}}^{m_{H^0}}$ is the same as that of $\Gamma_{h\to \mathrm{SM}}$, but m_h is replaced by m_{H^0}.

According to the observations of ATLAS [30] and CMS [31], the Higgs mass now is known to be $m_h = 125$ GeV, and the associated width is $\Gamma_{h\to \mathrm{SM}} = 4.21$ MeV [47]. Taking these values as inputs, we plot the contours for $\mathrm{BR}(h \to \chi\chi)$ as a function of $g_X \tan\theta$ and m_χ in the left panel of Fig. 1, where the solid line denotes the current upper limit of data with $\mathrm{BR}(h \to \chi\chi) < 0.29$ [48], and the region above the curve is excluded. Although the new scalar boson H^0 has not been observed yet and its mass is unknown, for completeness, we also show its invisible decay as a function of $g_X \cot\theta$ and m_χ in the right panel of Fig. 1 with the setting of $m_{H^0} = 2m_\chi + 1$ GeV, where the adopted mass relation $m_{H^0} \simeq 2m_\chi$ can explain the galactic center gamma ray excess [32].

Based on a previous investigation [32], it is known that the measured relic density of DM could bound the couplings of DM annihilating into SM particles; however, a stronger limit has arisen from the direct detection. By Eq. (11), we see that the coupling of each h and H^0 to χ is associated with s_θ and c_θ, respectively. Since their couplings to quarks are c_θ and s_θ, except the mass differences of intermedia, the spin-independent cross section of DM scattering off nucleons only depends on $g_X c_\theta s_\theta$ for both h and H^0. In terms of the results measured by the LUX Collaboration [2], we present the allowed values of $g_X s_\theta$ and m_X in Fig. 2, where the dashed and dotted lines stand for $m_{H^0} = m_\chi$ and $2m_\chi$, respectively. For comparison, we also show the situation for invisible Higgs decay $h \to \chi\bar{\chi}$. From the results, it can be seen that for $m_\chi < m_{h(H^0)}/2$ invisible Higgs decay gives the most restrictive limit. However, for $m_{H^0} \sim m_\chi$, the strongest bound is from the experiment of DM direct detection.

B. Signal processes and backgrounds

The signals of WIMPs in the model originate from the SM Higgs and new scalar H^0 decays, denoted by $S^{(*)} \to \chi\bar{\chi}$, in which scalar S can be on shell or off shell. The potential channels for producing DM pairs through the S portal are found to be (a) VBF, $pp \to S^{(*)}jj$, (b) monojet, $pp \to S^{(*)}j$, (c) mono-W/Z, $pp \to S^{(*)}W/Z$, and (d) $t\bar{t}$, $pp \to S^{(*)}t\bar{t}$. The monojet is the loop-induced process $gg \to S^{(*)}g$ [49,50]. In order to understand and estimate the production cross section of each channel, we implemented our model in CalcHEP [51] and utilized the code

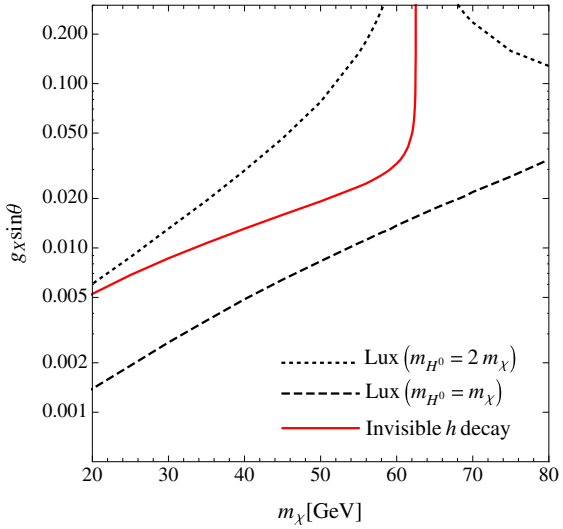

FIG. 2. Bounds of $g_X \sin\theta$ and m_χ from DM scattering off nucleons, where the red solid and black dashed (dotted) lines stand for the limits from the invisible SM Higgs decay and LUX experiment [2] with $m_{H^0} = m_\chi(2m_\chi)$, respectively.

with CTEQ6L PDF [52] and $\sqrt{s} = 14$ TeV to run numerical calculations.

Consequently, the production cross sections for $pp \to S^{(*)}X$, with X being the involved final state, are presented in Fig. 3, where the left panel is for on-shell H^0. Since the effect of on-shell h is similar to that of H^0, except for c_θ dependence instead of s_θ, here we only show the results of H^0. The right panel of Fig. 3 is for off-shell h and H^0. In this case, since m_χ and m_{H^0} are the explicit parameters in the processes, we adopt $m_{H^0} = m_\chi$ as the representative case. For reducing the dependence of this parameter, we scale the left and right panels by factors of $1/s_\theta^2$ and $1/(g_X^2 s_\theta^2 c_\theta^2)$, respectively. From these results, it can be clearly seen that monojet and VBF processes dominate the production cross section in the region of $m_{H^0} > 50$ GeV. Nevertheless, when we further impose the kinematic cuts for reducing the events of backgrounds, the contributions of monojet to the significance will become subleading effects. Hence, the main contributions to the signals are indeed from the VBF process, and thus, we focus our study on this channel. Additionally, from the plots, we also know that the off-shell processes are much smaller than those arising from the resonance of S.

Since DM candidates are invisible particles and the production mechanism at the LHC in the model is through VBF, the signal events at the detector level will appear as

$$2\,\text{jets} + \not{E}_T, \tag{16}$$

where $\not{E}_T$ is the missing transverse energy. As known, the background events generated from the SM contributions can also mimic the signal events of Eq. (16). In order to distinguish the signals from the backgrounds, we consider the following background processes [53]:

(1) Zjj background: $pp \to Zjj$,
(2) $Zjjj$ background: $pp \to Zjjj$,
(3) Wjj background: $pp \to W^\pm jj$,
(4) $Wjjj$ background: $pp \to W^\pm jjj$,
(5) top background: $pp \to tW^-\bar{b}(\bar{t}W^+b)$,

where the missing transverse energy $\not{E}_T$ is from the Z and W boson leptonic decays. Although charged leptons can be generated by W decays, when they are misidentified by the detectors, the events will appear as missing E_T. Similarly, this situation could also happen in jet. Therefore, for analyzing the backgrounds, when the events are generated, we set the number of jets in the final states to be up to three. We note that although QCD multijets are also the source of the background, however their contributions can be further reduced by the kinematic cuts.

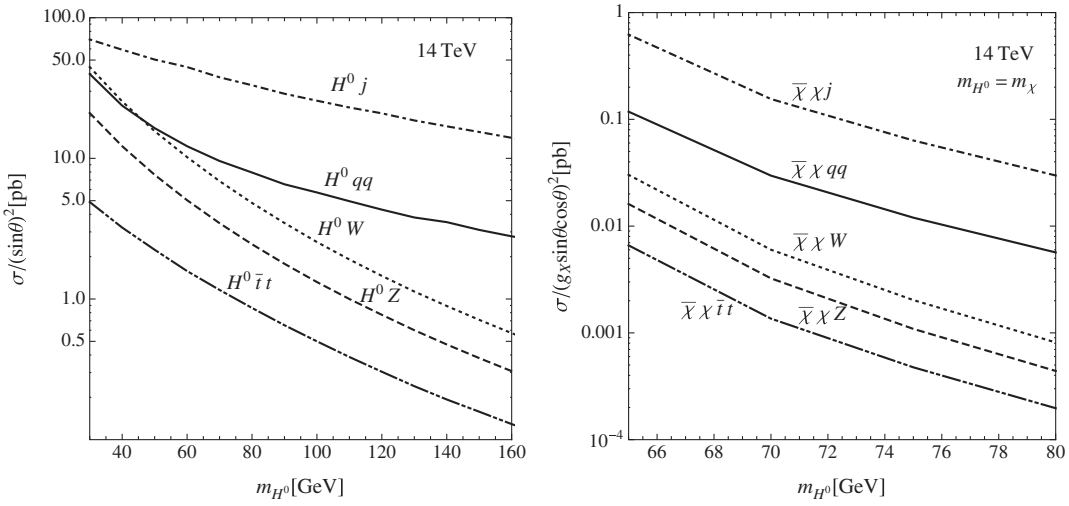

FIG. 3. Cross section of each signal channel for on-shell H^0 (left) and off-shell h and H^0 (right) as a function of m_{H^0}, where $\sqrt{s} = 14$ TeV is used, and for each panel, we scaled the cross section by factors of $1/\sin^2\theta$ and $1/(g_X^2 \sin^2\theta\cos^2\theta)$, respectively.

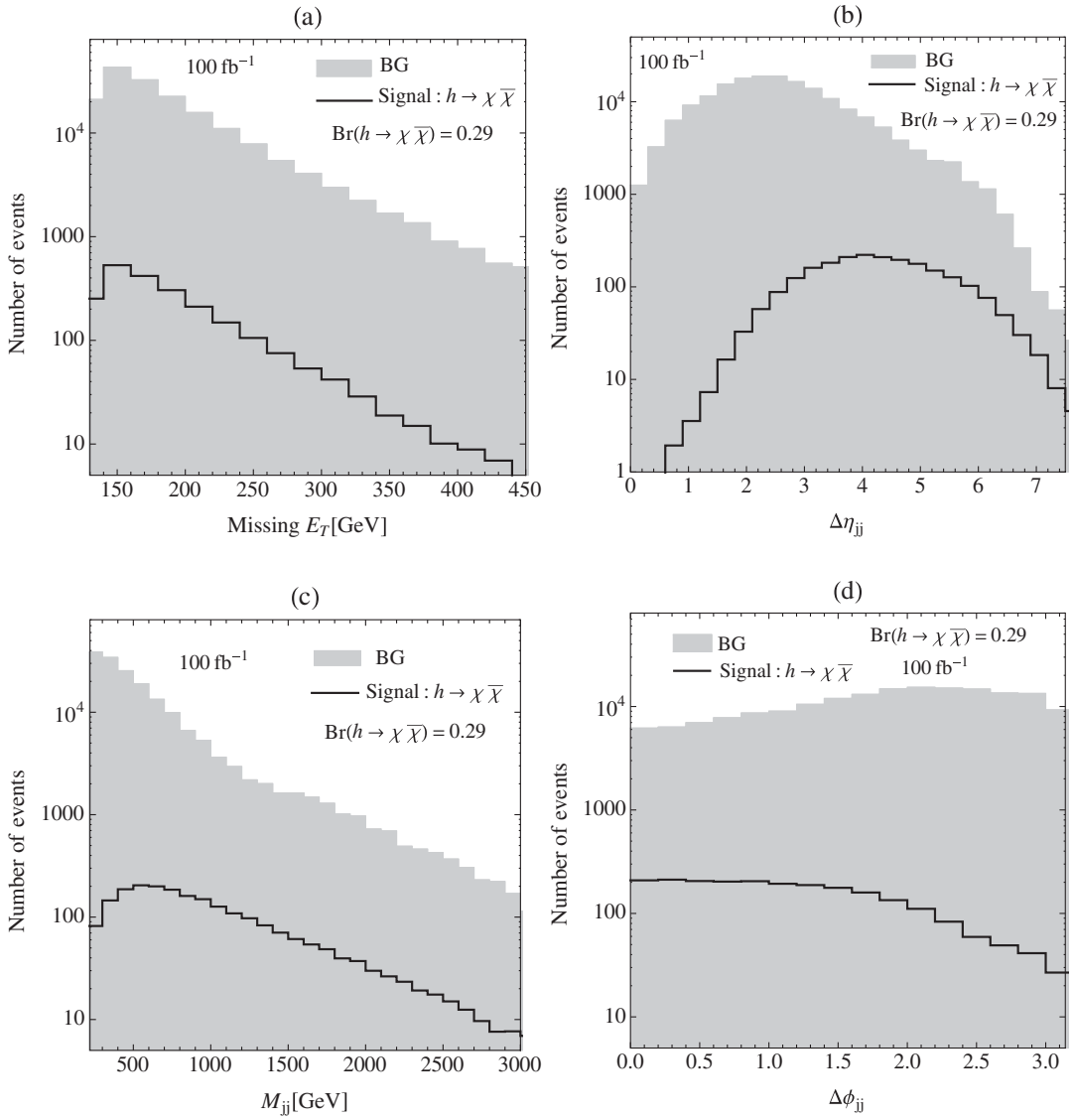

FIG. 4. Event histogram for $pp \to h(\chi\bar{\chi})qq$ and related background as a function of (a) missing E_T, (b) $\Delta\eta_{jj}$, (c) M_{jj}, and (d) $\Delta\phi_{jj}$, where the event selection criteria of Eq. (17) are adopted.

IV. EVENT SIMULATION AND DISCUSSIONS

After discussing the potential DM signals and possible backgrounds, we simulate the events by introducing proper kinematic cuts and investigate the resultant significance at $\sqrt{s} = 14$ TeV and luminosities of 100 and 300 fb^{-1}. As mentioned earlier, since the VBF process $pp \to S^{(*)}qq$ is the most promising mode to get a large ratio of the signal to background, in the following analysis, we only concentrate on VBF.

In order to perform the event simulation, we employ the event generator `MADGRAPH/MADEVENT 5` (MG5) [54] with `NNPDF23LO1` PDFs [55], where the necessary Feynman rules and relevant parameters of the model are created by `FeynRules 2.0` [56]. The generated events are further passed onto `PYTHIA 6` [57] to deal with the fragmentation of hadronic effects, the initial-state radiation (ISR) and final-state radiation (FSR) effects, and the decays of SM particles (e.g. Z boson, W boson, t quark, etc.). In addition, these events are also run through the `PGS 4` detector simulation [58].

A. Event selections and kinematic cuts

For enhancing the ratio of the signal to background, we propose proper criteria to suppress the backgrounds. Since Higgs portal DM production at the LHC has been studied in the literature [59,60] and the production mechanism also exists in our model, we first perform the DM production through the processes $pp \to hqq$ and invisible Higgs decay $h \to \chi\bar{\chi}$. Then, we can directly apply the event selections for an invisible Higgs search proposed by CMS [43] and set them as

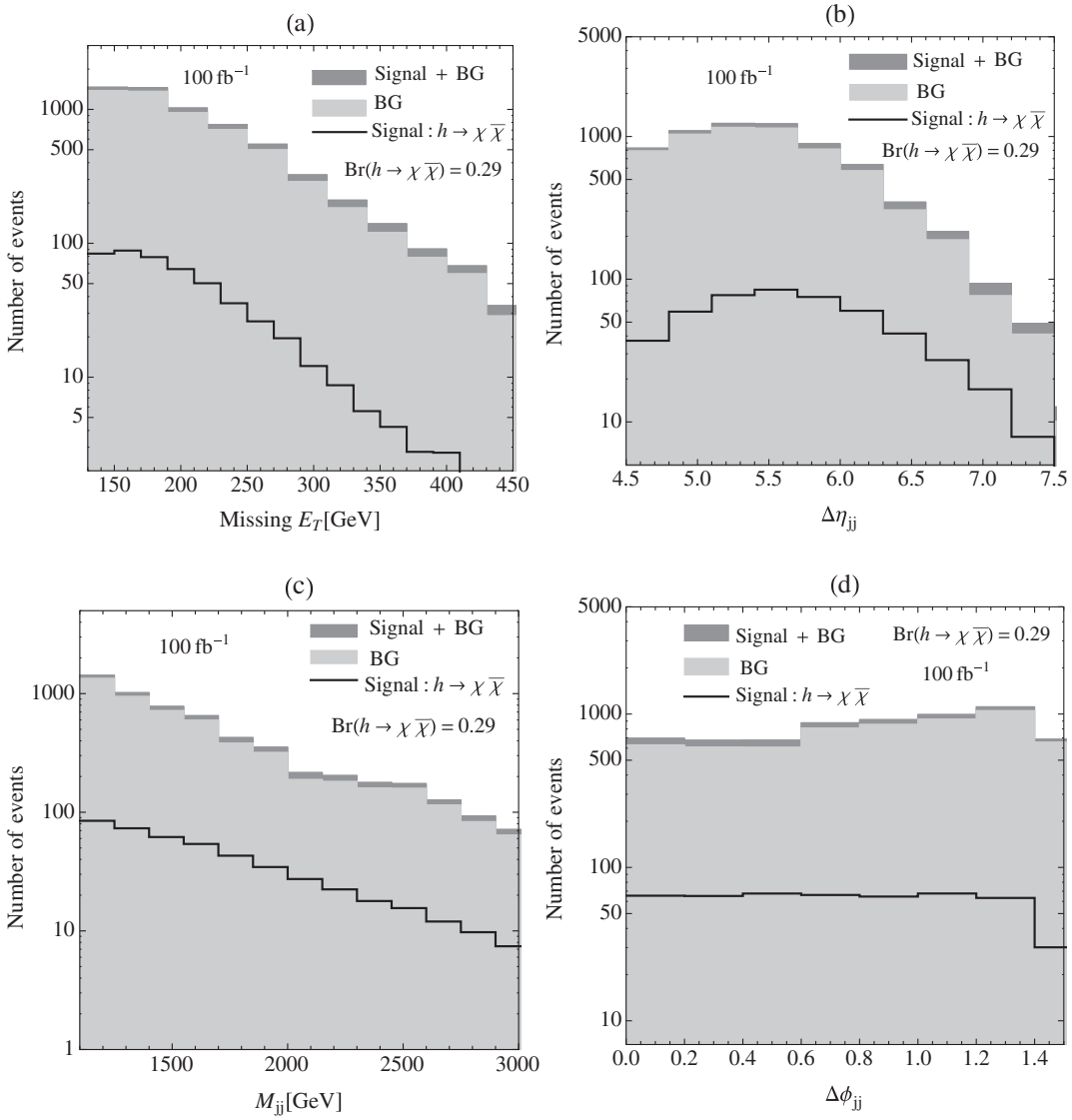

FIG. 5. The legend is the same as that in Fig. 4, but both basic and advanced cuts of Eqs. (17) and (18) are applied simultaneously.

$$p_T(j) > 50 \text{ GeV}, \quad |\eta(j)| < 4.7, \quad \eta(j_1)\cdot\eta(j_2) < 0,$$
$$\not{E}_T > 130 \text{ GeV}, \quad M_{jj} > 200 \text{ GeV}, \tag{17}$$

where $p_T(j)$ and $\eta(j)$ are the transverse momentum and pseudo-rapidity of jet j, and M_{jj} is the invariant mass of two jets. Although these conditions are used for collision energy at $\sqrt{s} = 7$ and 8 TeV in the CMS experiments, according to our MG5 event simulations, it is found that the distributions of jet p_T and $\not{E}_T$ indeed are not sensitive to the total collision energy of LHC. Therefore, in this study we take these selection conditions as the basic criteria for event kinematic cuts at $\sqrt{s} = 14$ TeV. Using the event generator MG5 and the cuts of Eq. (17), we show the histograms of the signal and background as a function of $\not{E}_T$, $\Delta\eta_{jj}$, M_{jj} and $\Delta\phi_{jj}$ in Figs. 4(a), 4(b), 4(c), and 4(d), respectively, where $\Delta\eta_{jj} = |\eta_{j_1} - \eta_{j_2}|$ and $\Delta\phi_{jj} = |\phi_{j_1} - \phi_{j_2}|$ are the pseudo-rapidity difference and azimuthal angle difference of the two-jet final state, respectively.

From the results of Fig. 4, we find that at low $\Delta\eta_{jj}$ background events are much larger than signals. If we further impose a cut on $\Delta\eta_{jj}$, the background events will be significantly reduced. Similar behavior also occurs at $M_{jj} < 1100$ GeV and $\Delta\phi_{jj} > 1.5$. Therefore, utilizing the difference in the kinematic region between the signal and background, we propose stricter event selection conditions on $\Delta\eta_{jj}$, M_{jj}, and $\Delta\phi_{jj}$, given as

$$\Delta\eta_{jj} > 4.5, \quad \Delta\phi_{jj} < 1.5, \quad M_{jj} > 1100 \text{ GeV}. \tag{18}$$

When both cuts of Eqs. (17) and (18) are imposed simultaneously, the resultant histograms as a function of $\not{E}_T$, $\Delta\eta_{jj}$, M_{jj}, and $\Delta\phi_{jj}$ are shown in Fig. 5.

TABLE I. Cross sections of signal and background (in units of fb) at $\sqrt{s} = 14$ TeV and at detector level, where the introduced kinematic cuts in Eqs. (17) and (18) were applied, $R_h = \cos^2\theta \mathrm{BR}(h \to \chi\bar{\chi})$, $R_{H^0} = \sin^2\theta \mathrm{BR}(H^0 \to \chi\bar{\chi})$, and $R_{\mathrm{off}} = (g_X \sin\theta\cos\theta)^2$. For the background, we present the cross sections after each cut, where the basic cuts are shown in Eq. (17).

		Zjj	$Zjjj$	Wjj	$Wjjj$
σ_{BG}[fb]	Basic cuts	2831.	705.	1315.	184.
	$+\Delta\eta_{jj}$	124.	33.8	50.6	7.73
	$+\Delta\phi_{jj}$	69.4	18.1	26.2	3.97
	$+M_{jj}$	32.9	8.54	14.2	2.20
σ_{S}[fb]	m_χ[GeV]	40	50	60	
	$\mathrm{I_A}$	$18.6\,R_{H^0} + 17.2\,R_h$	$17.5\,R_{H^0} + 17.2\,R_h$	$17.3\,R_{H^0} + 17.2\,R_h$	
	$\mathrm{I_B}$	$17.2\,R_h$	$17.2\,R_h$	$17.2\,R_h$	
	m_χ[GeV]	65	70	75	
	$\mathrm{II_A}$	$16.3\,R_{H^0}$	$16.0\,R_{H^0}$	$15.4\,R_{H^0}$	
	$\mathrm{II_B}$	$0.689\,R_{\mathrm{off}}$	$0.211\,R_{\mathrm{off}}$	$0.102\,R_{\mathrm{off}}$	

B. Discovery significance of signal

The event production of $pp \to S^{(*)}(\to \chi\bar{\chi})X$ depends on the mass of DM. For interpreting the gamma ray excess from the galactic center at the same time, we concentrate on the DM with $m_\chi < m_W$. For distinguishing the contributions of on-shell h from the off-shell one, we set the allowed range of m_χ to be the following two schemes:

$$\mathrm{I}:\ m_\chi < \frac{m_h}{2}, \qquad \mathrm{II}:\ \frac{m_h}{2} < m_\chi < m_W, \tag{19}$$

where the former dictates DM pair production to be through invisible Higgs decay while the latter dictates it to be through the Higgs propagator. Based on a previous study [32], for explaining the galactic center gamma ray excess via DM annihilation in this model, the favored ranges for m_{H^0} are $m_{H^0} \gtrsim 2m_\chi$ and $m_{H^0} \lesssim m_\chi$. In order to fit well with the gamma ray data, we find $m_{H^0} \sim 2m_\chi$ and $m_\chi \sim m_{H^0}$. For numerical calculations, we adopt the mass relation as

$$\mathrm{A}:\ m_{H^0} > 2m_\chi, \qquad \mathrm{B}:\ m_{H^0} < 2m_\chi \text{ GeV}. \tag{20}$$

Here, H^0 can decay into a DM pair in case A while case B is through off-shell H^0. Since $m_h = 125$ GeV is known and the unobserved m_{H^0} is still a free parameter, we investigate various situations by combining schemes I and II of Eq. (19) with cases A and B of Eq. (20), denoted as $\mathrm{I_A}$, $\mathrm{I_B}$, $\mathrm{II_A}$, and $\mathrm{II_B}$,

After setting up the kinematic cuts and classifying the possible schemes for m_χ and m_{H^0}, we calculate the cross sections of the background and signal with various values of m_χ in schemes $\mathrm{I_{A,B}}$ and $\mathrm{II_{A,B}}$. The numerical values are presented in Table I, where the simulated events had passed through PYTHIA 6 and PGS 4 detector simulation, and the cuts of Eqs. (17) and (18) were employed, $R_h = c_\theta^2 \mathrm{BR}(h \to \chi\bar{\chi})$, $R_{H^0} = s_\theta^2 \mathrm{BR}(H^0 \to \chi\bar{\chi})$, and $R_{\mathrm{off}} = (g_X s_\theta c_\theta)^2$. The associated cross section is obtained as

$$\sigma_{\mathrm{BG/S}} = \sigma_{\mathrm{BG/S}}^{\mathrm{MG5}} \frac{N_{\mathrm{cuts}}}{N_{\mathrm{tot}}}. \tag{21}$$

Here, $\sigma_{\mathrm{BG/S}}^{\mathrm{MG5}}$ is the cross section of the background/signal provided by MG5, N_{tot} is the number of original generated events and N_{cuts} is the number of selected events. For the background events, we have summed up all channels. We find that the dominant backgrounds are from Z + jets, where Z invisibly decays into neutrinos. By requiring null charged leptons in the final states, the event number from W + jets should be smaller than that from Z + jets. We also investigate the background associated with the top quark by generating event $tW^-\bar{b}(\bar{t}W^+b)$, which includes $t\bar{t}$ production. Since the corresponding cross section is less than 1 fb when event selections are applied, we do not show its value in Table. I. To understand the effect of kinematical cuts, we show the background cross section for each step of cuts, where the basic cuts are shown in Eq. (17). It can be clearly seen that $\Delta\eta_{jj}$ cuts reduce the background significantly.

For studying the potentiality of discovery, as typically done, we define the significance as $S = n_s/\sqrt{n_b}$, where n_s and n_b denote the numbers of selected events for the signal and background, respectively. For numerical illustration, we take $m_\chi = 50$ GeV for the schemes $\mathrm{I_{A,B}}$ and $m_\chi = 70$ GeV for schemes $\mathrm{II_{A,B}}$. Here, we adopt $m_H = m_\chi - 1$ GeV and $m_H = 2m_\chi + 1$ GeV for schemes $\{\mathrm{I_B}, \mathrm{II_B}\}$ and $\{\mathrm{I_A}, \mathrm{II_A}\}$, respectively. Accordingly, we display the discovery significance as a function of $g_X s_\theta$ with 100 and 300 fb^{-1} in Fig. 6. Since the sensitive regions of $g_X s_\theta$ are different in different schemes, we take the horizontal domain to be [0.002, 0.02], [0.05, 0.2], and [0.3, 3] for $\mathrm{I_{A,B}}$, $\mathrm{II_A}$ and $\mathrm{II_B}$, respectively.

For understanding the influence of g_X, we show the situations of $g_X = (0.05, 1.0)$ for scheme I_A and $g_X = (0.5, 1.0)$ for scheme $\mathrm{II_A}$. From the plots, it can be seen that when the value of $g_X s_\theta$ is fixed, the contributions of H^0 are smaller in schemes $\mathrm{I_A}$ if the value of g_X is larger. That is, H^0

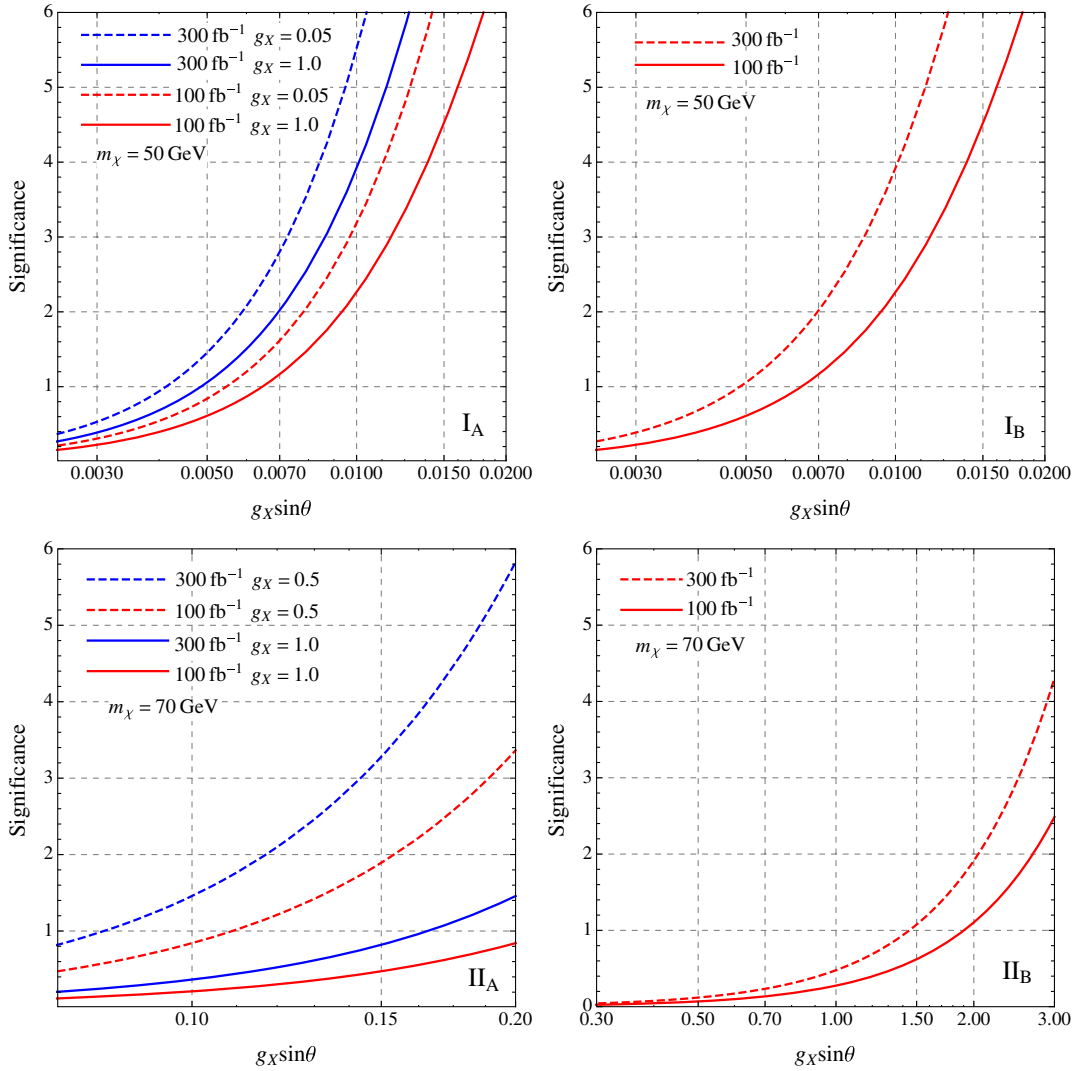

FIG. 6. Discovery significance as a function of $g_X \sin\theta$, where we set $m_\chi = 50$ GeV for $\mathrm{I_{A,B}}$ and $m_\chi = 70$ GeV for $\mathrm{II_{A,B}}$, and the luminosities of 100 and 300 fb^{-1} are used.

in $\mathrm{I_A}$ has a significant effect at small g_X or large s_θ values. Since H^0 is off shell in scheme $\mathrm{I_B}$ and its effect is negligible, by comparing the results of $\mathrm{I_A}$ with those of $\mathrm{I_B}$, one can determine the influence of on-shell H^0 on $\mathrm{I_A}$. Since h is an off-shell particle in scheme $\mathrm{II_A}$, the main contributions are from the invisible H^0 decays. According to Eq. (15) and the results of Fig. 1 and Table I, we need a somewhat larger value of $g_X s_\theta$ to get more signal events. Therefore, the domain of $g_X s_\theta$ is set to be 1 order of magnitude larger than that in $\mathrm{I_{A,B}}$. In scheme $\mathrm{II_B}$, the signal events are from off-shell h and H^0. Therefore, in order to enhance the signal events, we need a large value of $g_X s_\theta$. Unfortunately, when $S > 2$, g_X becomes a strong coupling constant. We thus omit the scheme $\mathrm{II_B}$ in the following discussions.

Furthermore, in order to understand the dependence of significance on the second Higgs mass, we investigate the significance by changing the value of m_H. We note that scheme $\mathrm{I_B}$ is independent of m_H as long as it satisfies $m_H < 2m_\chi$ because off-shell H^0 effects are negligible. We thus focus on schemes $\mathrm{I_A}$ and $\mathrm{II_A}$ here. The upper left (right) plot in Fig. 7 shows the contours in m_χ-$g_X \sin\theta$ plane with $S = 2(5)$. For $g_X = 0.05$, we take $m_H = 125$, 250 and 500 GeV. Due to the small $\sin\theta$, H^0 contributions are negligible, and the $g_X = 1$ case does not depend on m_H. It can be seen that if the value of $g_X \sin\theta$ is fixed, the significance increases with decreasing m_H. Moreover the effect of H^0 can be seen for $2m_\chi \sim m_h$, even though m_H is as heavy as 500 GeV. Also, the region with thick black lines is excluded from the analysis of the Higgs boson search at the LHC in Fig. 4 of Ref. [46]. The lower plot in Fig. 7 show the contours in the m_H- $\sin\theta$ plane with $S = 2$ and 5. Since the branching ratio for $H^0 \to \chi\bar{\chi}$ is $\sim$1, the significance in scheme $\mathrm{II_A}$ does not strongly depend on g_X when

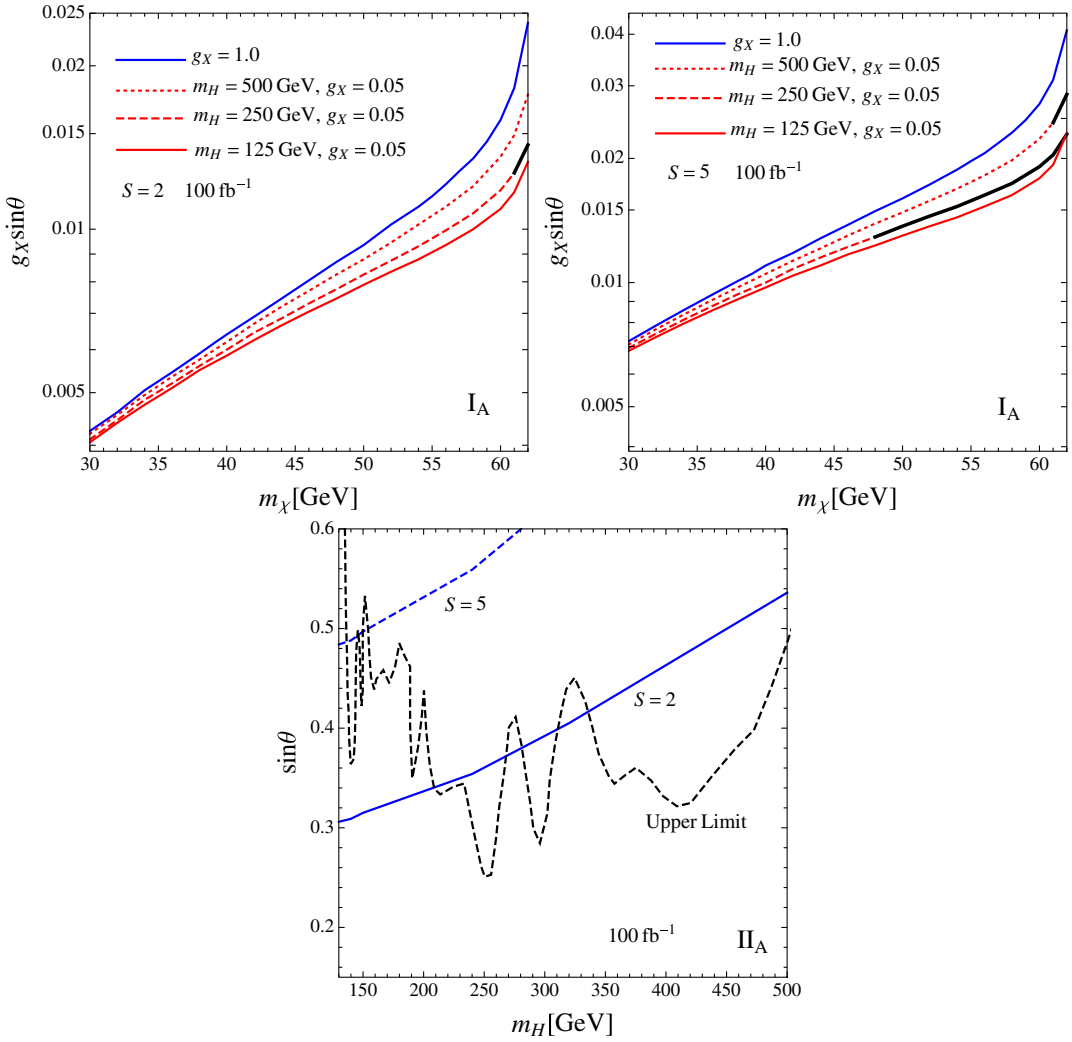

FIG. 7. The upper left (right) plot shows the correlation between $g_X \sin\theta$ and m_χ for $S = 2(5)$ in scheme I_A. The lower plot shows the correlation between $\sin\theta$ and m_H in scheme II_A. The upper limit of the mixing angle $\sin\theta$ is given from the analysis of the Higgs boson search at the LHC in Fig. 4 of Ref. [46]. The region with thick black lines for the scheme I_A is excluded by the constraint on $\sin\theta$.

$g_X \gtrsim 0.1$. Moreover the significance does not depend on m_χ as long as $m_H > 2m_\chi$ is satisfied. We also show the upper limit of $\sin\theta$, taken from Fig. 4 of Ref. [46], as a function of m_H. We find that the stronger constraint for $\sin\theta$ is in the higher m_H region.

After studying the potential for discovering DM signatures at the LHC, in order to further understand the relationship between significance and free parameters, we show the correlation between $g_X s_\theta$ and m_χ for schemes $I_{A,B}$ and II_A in Fig. 8. Since the significance in the situation of lower m_H and on-shell H^0 is larger, we also consider $m_H = 2m_\chi + 1$ GeV for schemes I_A and II_A. For illustration, we use 100 fb^{-1} and adopt $S = 2$ and $S = 5$ in the plots. Since the large $g_X s_\theta$ in scheme II_B is excluded by DM direct detection experiments, we do not further discuss the case. Additionally, the limit obtained from DM direct detection is also shown in the plots.

From the results in Fig. 8, it can be seen that the current invisible Higgs decay measured by ATLAS at $\sqrt{s} = 8$ TeV [48] cannot give a strict bound on the parameters of schemes I_A and I_B. Due to off-shell h, the data of invisible Higgs decay are not suitable for scheme II_A. Recalling the results in Fig. 2, since the constraint from the invisible Higgs decay in scheme $I_A(I_B)$ is stronger (weaker) than that from the LUX experiment, the significance over $S = 2$ with 100 fb^{-1} in scheme I_B is excluded by the current LUX data. For enhancing the significance of scheme I_B, a higher luminosity is necessary. Although the required values of $g_X s_\theta$ for $S = 5$ in scheme II_A are 1 order of magnitude larger than those in scheme I_B, for the case with $m_{H^0} = 2m_\chi + 1 > m_h$, $S = 5$ is still allowed, even though the limit of the LUX is considered. We conclude that schemes I_A and II_A have the highest discovery potential in our model.

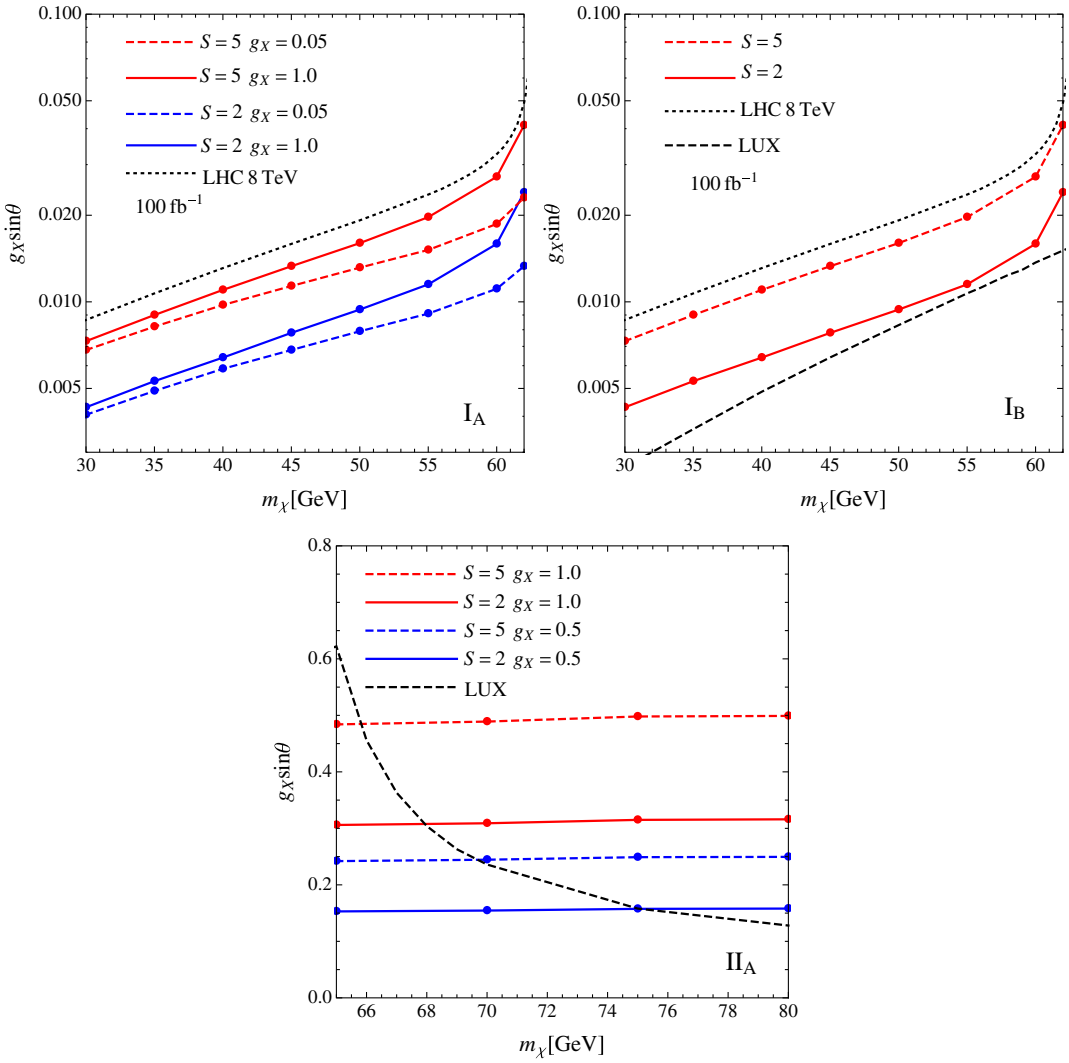

FIG. 8. Correlation between $g_X \sin\theta$ and m_χ for $S = 2$ and $S = 5$, where DM direct detection measured by the LUX Collaboration [2] is included, and the upper limit of invisible Higgs decay measured by ATLAS [48] at $\sqrt{s} = 8$ TeV is shown in schemes $\mathrm{I}_{\mathrm{A,B}}$.

V. CONCLUSION

A solution to the galactic center gamma ray excess is DM annihilation through the Higgs portal. We establish a Higgs portal model by considering a $SU(2)_X$ extension of the SM. We find that a Z_3 discrete symmetry is preserved when $SU(2)_X$ is broken spontaneously by the introduced quadruplet. Due to the residual Z_3 symmetry, the stable DM candidates in the model are the gauge bosons χ_μ and $\overline{\chi}_\mu$. Besides the SM Higgs h, we have an extra scalar H^0 from the quadruplet. Since the quartic term $\Phi_4^\dagger \Phi_4 H^\dagger H$ in the scalar potential leads to the mixture of h and H^0, the mixing angle θ plays an essential role in the connection between visible and invisible sectors and in DM relic density, DM direct detection, and gamma ray excess [32].

In this paper, we studied the potential of observing invisible WIMPs at the 14-TeV LHC. Since VBF dominates the signal process, we only focused on this channel in the investigation. As a result, the signal events at the detector level are 2-jet + $\not{E}_T$. The possible backgrounds are from $Z/W + n$-jet and $tW^-\overline{b}(\bar{t}W^+b)$ with $n = 2, 3$. In VBF, the DM pairs are produced by h and H^0 portals, where h and H^0 could be on shell or off shell, depending on the mass of DM. According to the mass of DM, we classify the interesting schemes to be $m_h/2 > m_\chi$, $m_h/2 < m_\chi < m_W$, $m_{H^0} > 2m_\chi$, and $m_{H^0} < 2m_\chi$, denoted as $\mathrm{I}_{\mathrm{A,B}}$ and $\mathrm{II}_{\mathrm{A,B}}$, where I (II) stands for on-shell (off-shell) Higgs h and A (B) is on-shell (off-shell) H^0.

We present the discovery significance of WIMPs with 100 and 300 fb^{-1} at $\sqrt{s} = 14$ TeV in Fig. 6, where the bound from DM direct detection was not applied. From the plots, it can be seen that the four schemes used for numerical estimations could all reach a significance of 5σ. However, in order to obtain a sizable significance,

e.g., $S > 2$, scheme $\mathrm{II_B}$ requires a strong coupling constant, which is excluded by the DM direct detection experiments.

Furthermore, in Fig. 7, we show the dependence of the significance on the H^0 mass by concentrating on schemes $\mathrm{I_A}$ and $\mathrm{II_A}$, where the produced H^0 is on shell. For $\mathrm{I_A}$, we find that the effect of H^0 would be seen for $2m_\chi \sim m_h$, even though m_H is as heavy as 500 GeV. For $\mathrm{II_A}$, since the parameters are strongly constrained by the Higgs boson search, we find that in order to get $S > 2$ lighter H^0 is preferred for $\sin\theta$ to be large.

In Fig. 8, we show the correlation between $g_X \sin\theta$ and m_X for $S = 2$ and $S = 5$ in $\mathrm{I_{A,B}}$ and $\mathrm{II_A}$, where the limit from LUX experiments is included. In the plots, we just use 100 fb^{-1} as the representative value. From the results, we find that the values of parameters for $S = 5$ in schemes $\mathrm{I_A}$ and $\mathrm{II_A}$ could satisfy the bound of the LUX experiments. Hence, the proposed DM scalar portal model could be tested by the data of the 14-TeV LHC.

ACKNOWLEDGMENTS

This work is supported by the Ministry of Science and Technology of R.O.C. under Grants No. MOST-103-2112-M-006-004-MY3 (C. H. C.) and No. MOST-103-2811-M-006-030 (T. N.).

[1] K. A. Olive (Particle Data Group), Chin. Phys. C **38**, 090001 (2014).
[2] D. S. Akerib *et al.* (LUX Collaboration), Phys. Rev. Lett. **112**, 091303 (2014).
[3] O. Adriani *et al.* (PAMELA Collaboration), Nature (London) **458**, 607 (2009).
[4] M. Ackermann *et al.* (Fermi LAT Collaboration), Phys. Rev. Lett. **108**, 011103 (2012).
[5] L. Accardo *et al.* (AMS Collaboration), Phys. Rev. Lett. **113**, 121101 (2014).
[6] M. Aguilar *et al.* (AMS Collaboration), Phys. Rev. Lett. **113**, 221102 (2014).
[7] D. Hooper, P. Blasi, and P. D. Serpico, J. Cosmol. Astropart. Phys. 01 (2009) 025; H. Yuksel, M. D. Kistler, and T. Stanev, Phys. Rev. Lett. **103**, 051101 (2009); S. Profumo, Central Eur. J. Phys. **10**, 1 (2011); D. Malyshev, I. Cholis, and J. Gelfand, Phys. Rev. D **80**, 063005 (2009).
[8] D. Grasso *et al.* (FERMI-LAT Collaboration), Astropart. Phys. **32**, 140 (2009); T. Linden and S. Profumo, Astrophys. J. **772**, 18 (2013); P.-F. Yin, Z.-H. Yu, Q. Yuan, and X.-J. Bi, Phys. Rev. D **88**, 023001 (2013).
[9] K. Blum, B. Katz, and E. Waxman, Phys. Rev. Lett. **111**, 211101 (2013).
[10] L. Goodenough and D. Hooper, arXiv:0910.2998.
[11] D. Hooper and L. Goodenough, Phys. Lett. B **697**, 412 (2011).
[12] A. Boyarsky, D. Malyshev, and O. Ruchayskiy, Phys. Lett. B **705**, 165 (2011).
[13] D. Hooper and T. Linden, Phys. Rev. D **84**, 123005 (2011).
[14] K. N. Abazajian and M. Kaplinghat, Phys. Rev. D **86**, 083511 (2012); **87**, 129902(E) (2013).
[15] C. Gordon and O. Macias, Phys. Rev. D **88**, 083521 (2013); **89**, 049901(E) (2014).
[16] O. Macias and C. Gordon, Phys. Rev. D **89**, 063515 (2014).
[17] K. N. Abazajian, N. Canac, S. Horiuchi, and M. Kaplinghat, Phys. Rev. D **90**, 023526 (2014).
[18] V. Vitale *et al.* (Fermi/LAT Collaboration), *Proceedings of the 2009 Fermi Symposium, Washington, DC, 2009*, eConf C091122 (2009).
[19] A. Morselli *et al.* (Fermi-LAT Collaboration), Nuovo Cimento C **034N3**, 311 (2011).
[20] T. Daylan, D. P. Finkbeiner, D. Hooper, T. Linden, S. K. N. Portillo, N. L. Rodd, and T. R. Slatyer, Phys. Dark Univ. **12**, 1 (2016).
[21] B. Zhou, Y. F. Liang, X. Huang, X. Li, Y. Z. Fan, L. Feng, and J. Chang, Phys. Rev. D **91**, 123010 (2015).
[22] F. Calore, I. Cholis, and C. Weniger, J. Cosmol. Astropart. Phys. 03 (2015) 038.
[23] K. N. Abazajian, N. Canac, S. Horiuchi, M. Kaplinghat, and A. Kwa, J. Cosmol. Astropart. Phys. 07 (2015) 013.
[24] F. Calore, I. Cholis, C. McCabe, and C. Weniger, Phys. Rev. D **91**, 063003 (2015).
[25] J. D. Ruiz-Alvarez, C. A. de S.Pires, F. S. Queiroz, D. Restrepo, and P. S. Rodrigues da Silva, Phys. Rev. D **86**, 075011 (2012).
[26] Y. Farzan and A. R. Akbarieh, J. Cosmol. Astropart. Phys. 10 (2012) 026.
[27] A. Alves, S. Profumo, F. S. Queiroz, and W. Shepherd, Phys. Rev. D **90**, 115003 (2014).
[28] A. Berlin, P. Gratia, D. Hooper, and S. D. McDermott, Phys. Rev. D **90**, 015032 (2014).
[29] B. Patt and F. Wilczek, arXiv:hep-ph/0605188.
[30] G. Aad *et al.* (ATLAS Collaboration), Phys. Lett. B **716**, 1 (2012).
[31] S. Chatrchyan *et al.* (CMS Collaboration), Phys. Lett. B **716**, 30 (2012).
[32] C. H. Chen and T. Nomura, Phys. Lett. B **746**, 351 (2015).
[33] T. Hambye, J. High Energy Phys. 01 (2009) 028.
[34] C. W. Chiang, T. Nomura, and J. Tandean, J. High Energy Phys. 01 (2014) 183.
[35] C. Boehm, M. J. Dolan, and C. McCabe, Phys. Rev. D **90**, 023531 (2014).
[36] V. V. Khoze and G. Ro, J. High Energy Phys. 10 (2014) 61.
[37] S. Baek, P. Ko, and W. I. Park, J. Cosmol. Astropart. Phys. 10 (2014) 067.
[38] C. Gross, O. Lebedev, and Y. Mambrini, J. High Energy Phys. 08 (2015) 158.

[39] S. Di Chiara and K. Tuominen, J. High Energy Phys. 11 (2015) 188.
[40] G. Belanger, B. Dumont, U. Ellwanger, J. F. Gunion, and S. Kraml, Phys. Lett. B **723**, 340 (2013).
[41] A. Greljo, J. Julio, J. F. Kamenik, C. Smith, and J. Zupan, J. High Energy Phys. 11 (2013) 190.
[42] G. Aad *et al.* (ATLAS Collaboration), Phys. Rev. Lett. **112**, 201802 (2014).
[43] S. Chatrchyan *et al.* (CMS Collaboration), Eur. Phys. J. C **74**, 2980 (2014).
[44] M. Endo and Y. Takaesu, Phys. Lett. B **743**, 228 (2015).
[45] N. Craig, H. K. Lou, M. McCullough, and A. Thalapillil, J. High Energy Phys. 02 (2016) 127.
[46] T. Robens and T. Stefaniak, Eur. Phys. J. C **75**, 104 (2015).
[47] S. Heinemeyer *et al.* (LHC Higgs Cross Section Working Group Collaboration), arXiv:1307.1347.
[48] The ATLAS Collaboration, Reports No. ATLAS-CONF-2015-004 and No. ATLAS-COM-CONF-2015-004.
[49] J. Goodman, M. Ibe, A. Rajaraman, W. Shepherd, T. M. P. Tait, and H. B. Yu, Phys. Rev. D **82**, 116010 (2010).
[50] P. J. Fox, R. Harnik, J. Kopp, and Y. Tsai, Phys. Rev. D **85**, 056011 (2012).
[51] A. Belyaev, N. D. Christensen, and A. Pukhov, Comput. Phys. Commun. **184**, 1729 (2013).
[52] P. M. Nadolsky, H. L. Lai, Q. H. Cao, J. Huston, J. Pumplin, D. Stump, W. K. Tung, and C.-P. Yuan, Phys. Rev. D **78**, 013004 (2008).
[53] D. Ghosh, R. Godbole, M. Guchait, K. Mohan, and D. Sengupta, Phys. Lett. B **725**, 344 (2013).
[54] J. Alwall, R. Frederix, S. Frixione, V. Hirschi, F. Maltoni, O. Mattelaer, H.-S. Shao, T. Stelzer, P. Torrielli, and M. Zaro, J. High Energy Phys. 07 (2014) 079.
[55] C. S. Deans (NNPDF Collaboration), arXiv:1304.2781.
[56] A. Alloul, N. D. Christensen, C. Degrande, C. Duhr, and B. Fuks, Comput. Phys. Commun. **185**, 2250 (2014).
[57] T. Sjostrand, S. Mrenna, and P. Z. Skands, J. High Energy Phys. 05 (2006) 026.
[58] http://www.physics.ucdavis.edu/~conway/research/software/pgs/pgs4-general.htm.
[59] A. Djouadi, O. Lebedev, Y. Mambrini, and J. Quevillon, Phys. Lett. B **709**, 65 (2012).
[60] A. Djouadi, A. Falkowski, Y. Mambrini, and J. Quevillon, Eur. Phys. J. C **73**, 2455 (2013).